Bulletin of the New Zealand Society for Earthquake Engineering, Vol. 50, No. 4, December 2017

SEISMIC PERFORMANCE OF REPAIRED LIGHTLY-REINFORCED CONCRETE WALLS

Christopher J. Motter[1], Aaron B. Clauson[2], James C. Petch[3], Matias A. Hube[4], Richard S. Henry[5] and Kenneth J. Elwood[6]

(Submitted *March 2017*; Reviewed *August 2017*; Accepted *October 2017*)

ABSTRACT

As a result of the 2010-2011 Canterbury earthquakes, over 60% of the concrete buildings in the Christchurch Central Business District have been demolished. This experience has highlighted the need to provide guidance on the residual capacity and repairability of earthquake-damaged concrete buildings. As limited testing has been performed on repaired components, this study focuses on the performance of severely-damaged lightly-reinforced concrete walls repaired through replacement of reinforcement and concrete in the damaged region. The damage prior to repair included buckling and fracture of longitudinal reinforcement, crushing and spalling of concrete, and, for one of the two specimens, out-of-plane instability of the gross section. Prior to repairing the wall specimens, tensile testing of reinforcement with welded connections was conducted to verify acceptable performance of welds suitable for reinstating the damaged reinforcement. Repairs to the specimens consisted of removal of damaged concrete through either hydro-demolition or jack hammering, followed by cutting and removal of damaged reinforcement and reinstatement of new reinforcement and repair mortar. The two repaired wall specimens were tested using a standard protocol that was identical to that used for one of the two original wall specimens. Aside from a difference in the elastic stiffness, the load-deformation responses of the repaired specimens were similar to that of the originally-tested specimen through to the first loading cycle at 2.0% drift, beyond which strength degradation was more pronounced for the repaired specimens. The overall performance of the repaired walls relative to the original wall indicates that it is feasible to achieve acceptable performance of severely-damaged concrete walls repaired through replacement of reinforcement and concrete in the damaged region.

INTRODUCTION

The 2010-2011 Canterbury earthquakes in New Zealand resulted in more than $NZ 40 billion in losses and demolition of approximately 60% of the multi-storey concrete buildings due to the widespread damage and closure of the Christchurch Central Business District for more than two years [1]. During the recovery and rebuild phase for Christchurch it has become apparent that there are a number of factors that influence the post-earthquake decision of whether to repair or demolish a damaged structure. The decision depends not only on the current damage state of the structure but also on the assessment of residual seismic capacity and a cost benefit analysis of the different alternatives. Previous studies have stated that repair of the structure can be more economical than demolishing a building despite severe structural damage [2]. However, recent studies surrounding the Canterbury earthquakes have found that a significant number of modern multi-storey buildings that had a low damage ratio (where the damage ratio is the estimated cost of repair compared to cost of replacement of a structure) were deemed uneconomic to repair, declared a total insurance loss, and consequently demolished [1]. This is in part due to limited guidance currently provided on the repairability of structures, which has resulted in significant debate and litigation post-earthquake. Specific research is required to provide evidence of the seismic behaviour of repaired reinforced concrete components and buildings to remove the uncertainty surrounding the topic. While most ongoing research related to repairability has focused on relatively lightly-damaged components (e.g., [3, 4]), this study focuses on the feasibility of repairing severely-damaged components to assess if acceptable structural performance can be reinstated. Significant damage to reinforced concrete walls was observed after the 2011-2010 Canterbury, New Zealand earthquakes [5-7] and after the 2010 Maule, Chile earthquake [8, 9]. This damage included buckling of longitudinal reinforcement, crushing and spalling of concrete, and/or buckling of the global wall section in the out-of-plane direction. For this study, repair and retesting was carried out for two lightly-reinforced concrete walls that had different levels of damage prior to repair but were otherwise identical.

EXAMPLES OF REPAIRS OF EARTHQUAKE-DAMAGED STRUCTURES

This section briefly summarises repair techniques used on concrete buildings in Christchurch and Chile. In an effort to better understand the decision-making process used by building owners to determine whether to demolish or repair buildings, Marquis et al. [1] conducted case studies for multi-storey concrete buildings damaged in the 2010-2011 Canterbury earthquakes, eight of which were demolished and seven of which were repaired. Of the seven buildings that were repaired, two buildings, namely Building R113 and Building R163, had sustained a level of structural damage that required replacement of reinforcement and/or concrete.

[1] *Corresponding Author, Assistant Professor, Washington State University, Pullman, c.motter@wsu.edu (Member)*
[2] *Graduate Structural Engineer, Holmes Consulting, Auckland*
[3] *Structural Engineer, BGT Structures, Auckland*
[4] *Associate Professor, Pontificia Universidad Católica de Chile, Santiago, mhube@ing.puc.cl*
[5] *Senior Lecturer, University of Auckland, Auckland, rs.henry@auckland.ac.nz (Member)*
[6] *Professor, University of Auckland, Auckland, k.elwood@auckland.ac.nz (Member)*

Building R113 is a 19-storey moment frame building constructed in 1988. Structural damage included flexural cracking of beams and columns, shear cracking and loss of bond in precast pre-stressed floor ribs, spalling of concrete at the base of columns, cracking in floor slabs with residual crack widths as large as 4.0 mm, damage to steel beams due to the collapse of stairs, and failure of two RC columns in the carpark [10]. Repair included epoxy injection of cracks where possible. The damaged precast pre-stressed floor ribs were removed and new ribs and topping slabs were reinstated, with new reinforcement spliced to existing reinforcement with conventional straight bar laps. Spalled concrete in columns was repaired by breaking back to sound concrete and reinstating with repair mortar. For the large cracks in the floor around columns, the concrete slab was broken out in the region of severe cracking, and reinforcement and concrete were then reinstated, with new reinforcement lap spliced to existing reinforcement. Approximately 50% of the 3-level podium structure outside the footprint of the main tower footprint (the most significantly damaged part of the building apart from the stairs) was demolished and re-instated. Existing concrete podium columns within the retained part of the podium were concrete jacketed and/or FRP wrapped. Corner tower columns were strengthened with additional concrete jacketing and FRP wrapping. New concrete stairs with revised sliding movement joints were installed within the existing stair cores.

Building R163, constructed from 2002-2004, is comprised of an eight-storey east tower and a seven-storey west tower. The seismic force resisting system in both towers consists of structural walls in the basement, precast structural walls in the lower and middle stories, and steel frames in the upper stories. Structural damage included spalling of concrete and hairline cracking in walls and floors in addition to compression failure at end regions of structural walls at ground level. According to the owner of the building, the repair costs were initially estimated as 55% of the building value but increased to 90% of the building value when one part of the building was demolished and rebuilt [10]. In addition to epoxy injection of cracks, repairs to reinforced concrete walls included reinstatement of spalled concrete with structural mortar. Infill walls were cast with anchorage inserts used to anchor the new longitudinal reinforcement to existing structural walls above and below and “letterbox” openings in formwork used to pour concrete.

Demolition of reinforced concrete buildings following the 2010 Maule, Chile earthquake was less widespread than for the 2010-2011 Canterbury, New Zealand earthquakes. Four out of 12 buildings taller than ten stories that suffered substantial damage in Viña del Mar were demolished, while six of 23 damaged buildings in Concepción were demolished. Damage and repair procedures for two buildings in Chile after the 2010 earthquake are summarized below.

An 11-story (plus basement) concrete wall building in Viña del Mar suffered flexural compression failure of basement walls with crushing of concrete and buckling of longitudinal reinforcement [11]. Additionally, severe damage occurred in the joints of vertical and horizontal segments of walls with openings. The building was evacuated after the 2010 earthquake. Repair of this building included replacement of damaged concrete and buckled reinforcement (Figure 1a), cross-section enlargement of columns, strengthening of wall boundary elements with longitudinal and transverse reinforcement, and strengthening of wall webs with carbon fibre reinforced polymer (CFRP). The repair cost was approximately 1/3 of the cost of constructing a new building, and the cost of structural element repair was approximately 40% of the total repair cost.

Repairs to an 18-story structural wall building in Santiago, Chile are summarized by Sherstobitoff et al [12]. Following the 2010 earthquake, three structural walls had failed in flexural compression just below grade, causing downward vertical displacement of the grade-level floor and lateral displacement of the building. Jacking and shoring were used to support damaged structural walls during repair (Figure 1b). Instruments were installed and used to measure strains in structural walls during jacking, with fibre reinforced plastic (FRP) fabric used to mitigate the formation of new cracks. Existing cracks in structural walls were epoxy injected. Jacking was successfully used to reposition the building, and the building was re-opened for occupancy, with the total repair cost estimated as 25% of the cost to demolish and re-build.

These examples demonstrate a variety of methods used to repair structural concrete after earthquakes, including full reinstatement of critical zones of structural elements. The current study aims to demonstrate the seismic performance of severely damaged concrete walls repaired through reinstatement of a portion or the entire plastic hinge zone.

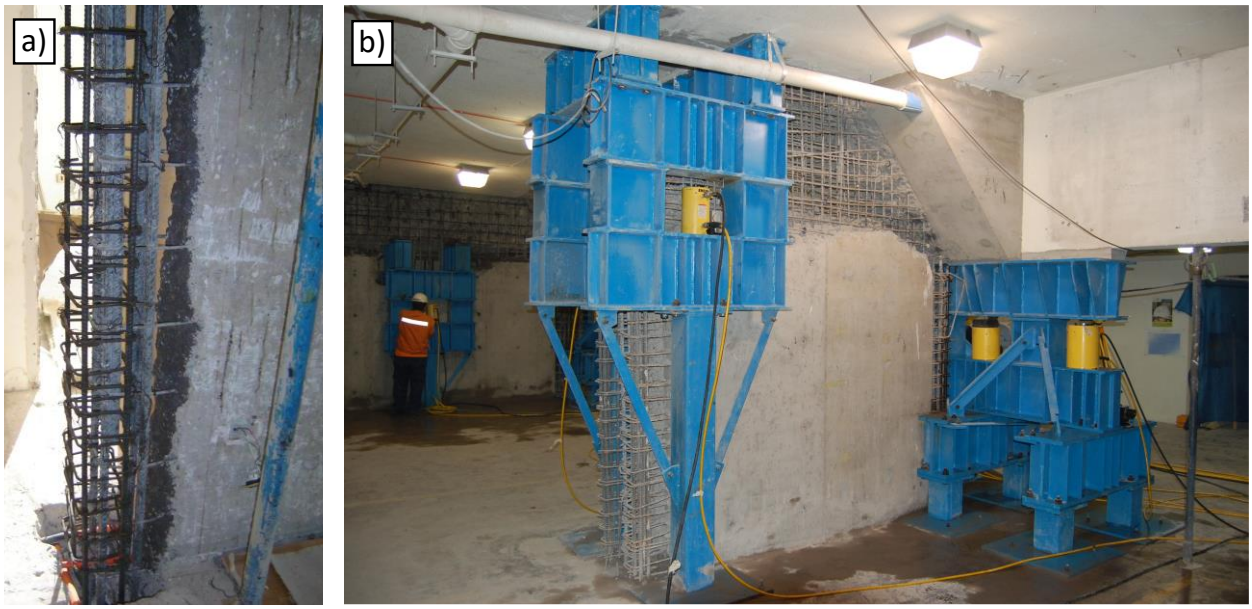

Figure 1: Repair of reinforced concrete walls after 2010 Maule, Chile earthquake: a) 11-storey building in Viña del Mar (photo courtesy of Jorge Carvallo); b) 18-storey building in Santiago (photo courtesy of John Sherstobitoff).

Table 1: Test matrix for tensile testing of reinforcement connections without concrete.

No. of Spec.	Connection	Reinf.	Drawing	Min. Eff. Length of Weld	Min. Size of Weld (S)	Min. Width of Weld (W)	Electrode	Weld Position	Current	Pre/ Post Heat
2	Straight Bar	HD10		N.A.	N.A.	N.A.	N.A.	N.A.	N.A.	N.A.
2	Straight Bar	HD16		N.A.	N.A.	N.A.	N.A.	N.A.	N.A.	N.A.
3	Double lap splice	HD10	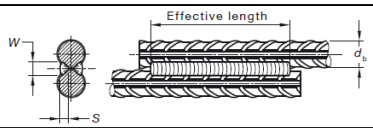	$5d_b$	$0.25d_b$	$0.45d_b$	AS/NZS 4857 B-E7618-GA H5 (P118)	Long.	100A	Pre Heat ~100°C
3	Double lap splice	HD16	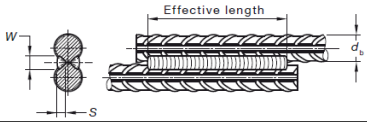	$5d_b$	$0.25d_b$	$0.45d_b$	AS/NZS 4857 B-E7618-GA H5 (P118)	Long.	100A	Pre Heat ~100°C
1	Indirect butt splice	HD16	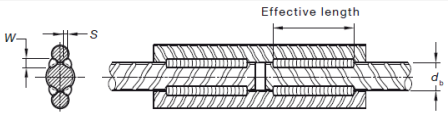	$3d_b$	$0.25d_b$	$0.45d_b$	AS/NZS 4857 B-E7618-GA H5 (P118)	Long.	100A	Pre Heat ~100°C
3	Ancon MBT coupler	HD16		N.A.	N.A.	N.A.	N.A.	N.A.	N.A.	N.A.

TESTING OF REINFORCEMENT CONNECTIONS

Repair of damaged reinforced concrete walls may involve removal and replacement of damaged reinforcement and concrete. As it is undesirable to remove more damaged material than necessary, it may not be practical to expose sufficiently long lengths of undamaged longitudinal reinforcement such that new reinforcement may be lap spliced to existing reinforcement in accordance with development length requirements of current design standards. Therefore, alternative means of connecting the new reinforcement to existing reinforcement were explored in this study. Tensile testing was conducted on reinforcement with the connection details shown in Table 1. These connection details included mechanical couplers (Ancon MTB couplers) in addition to welded connections. For the welded connections, various weld types and configurations were considered, including double lap splices that create an eccentric connection between the two bars being joined and indirect butt splices in which two short lengths of bar were lapped and welded along opposite sides of the two bars being connected. Straight bars, i.e., bars with no connections, were also included in the tensile testing to provide a baseline. It is noted that welding of reinforcing steel is permitted as per Structural Steel Welding Part 3: Welding of Reinforcing Steel [13].

During tensile testing of reinforcement, average reinforcement strains were measured over a 150 mm gage length using an extensometer that was not positioned across the connection. It is evident from the results of tensile testing of the reinforcement connections, shown in Figure 2, that the use of Ancon MTB couplers and indirect butt splices generally did not lead to an appreciable reduction in fracture strain of the reinforcement relative to the results obtained for straight bars. Double lap slices had a significantly reduced fracture strain in some instances. This reduction in performance was likely due to bending of the eccentric connection, shown in Figure 3. Fracture occurred at the welded connections of the double lap splices in some instances (e.g., Figure 3) but did not occur at the connection location for any other connection types. Therefore, based on the results obtained from this study, Ancon MTB couplers or welded indirect butt splices were considered for use in repair. Welded indirect butt splices were selected for use in the wall repairs described in the following section, as the connection was less bulky than that of the Ancon MTB coupler.

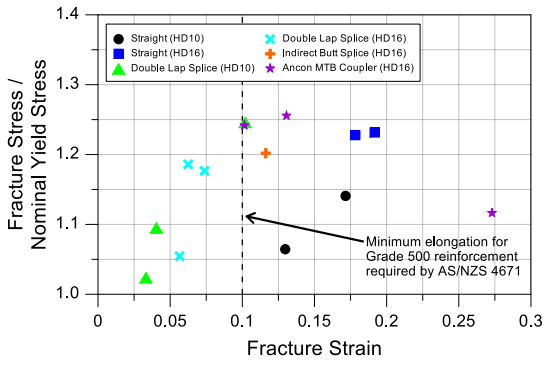

Figure 2: Results from tensile testing of reinforcement connections.

Figure 3: Fracture of double lap splice at weld.

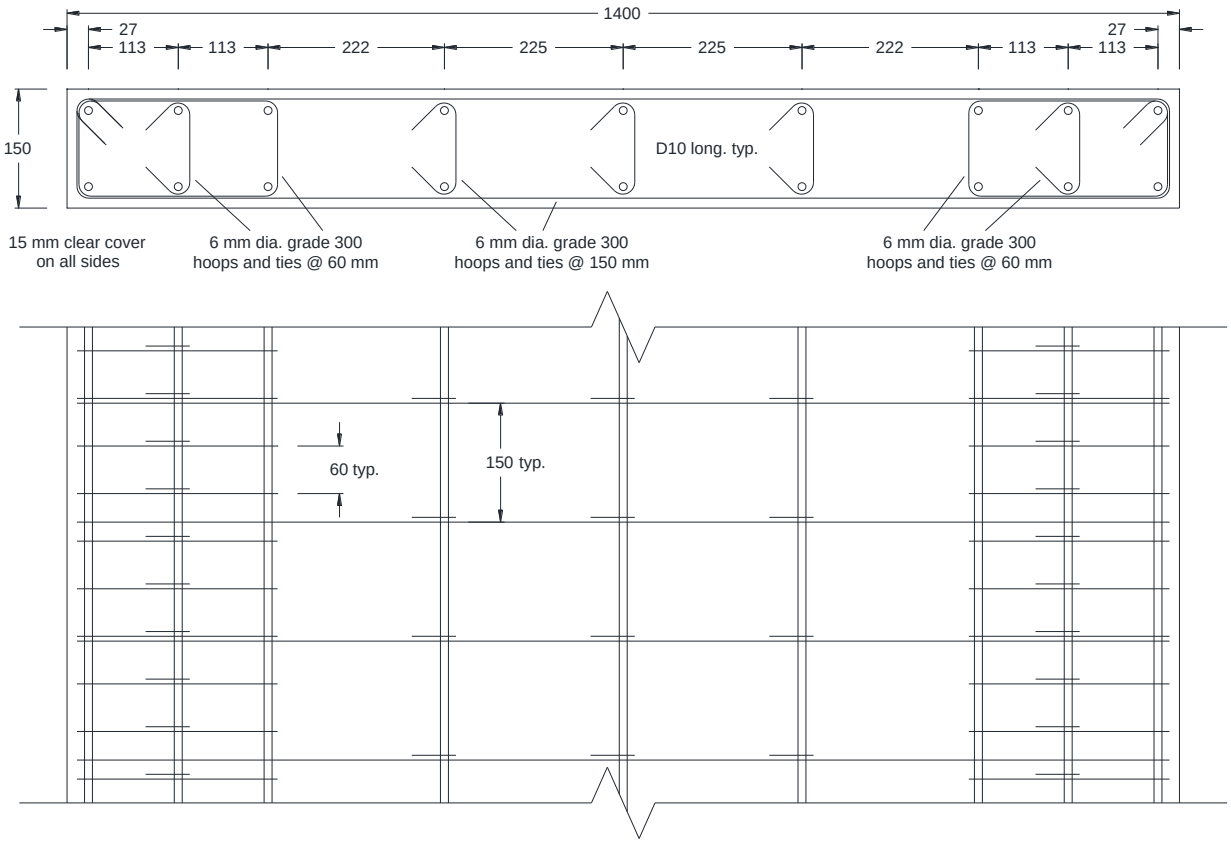

Figure 4: Wall cross-section and partial elevation (dimensions in mm).

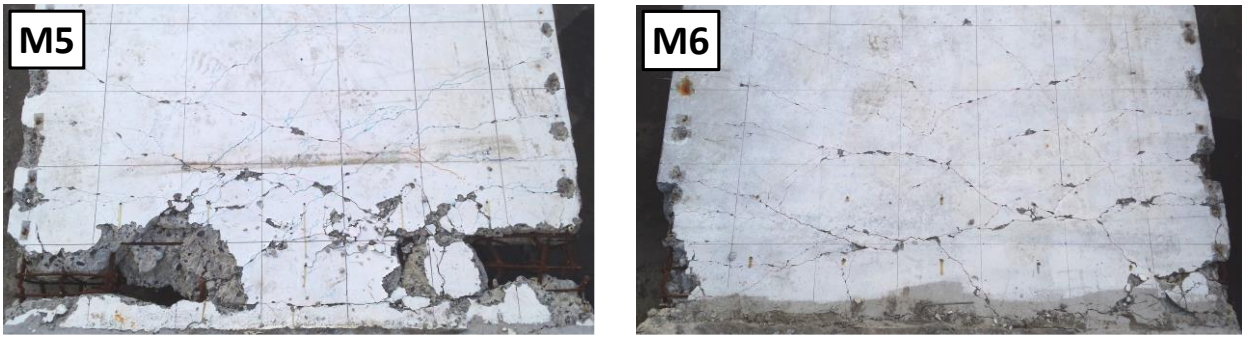

Figure 5: Damage of original specimens at the base of the wall after the completion of testing.

TEST SPECIMENS

The two test specimens that were repaired and re-tested in this study were lightly-reinforced concrete walls that were tested previously as part of a separate study [14]. The two specimens have identical wall cross-sections, as shown in Figure 4, with longitudinal reinforcement ratios of ρ = 0.005 in the web and ρ = 0.011 in the end regions. The original specimens are referred to as M5 and M6, while the repaired specimens are differentiated from the original specimens as M5-R and M6-R, respectively. M5-R and M6-R differed in the extent of damage from previous testing and in the repair techniques used. During testing of the original specimens (using the set-up described in the following section of this paper), wall M5 was tested to failure under a quasi-static, standard laboratory reversed cyclic protocol, while wall M6 was tested under demands that were analytically-determined to simulate the response of the wall to a specific earthquake. The difference in testing protocol resulted in different levels of damage at the completion of testing of the original specimens, as shown in Figure 5. M5 sustained significant damage that included buckling and fracture of longitudinal reinforcement, crushing and spalling of concrete, and instability of the global section in the out-of-plane direction. Damage was less extensive for M6 and included crushing and spalling of concrete and buckling of longitudinal reinforcement at the wall end regions.

Given the difference in the level of damage for the two walls prior to repair, a different approach to repair was taken for the two specimens. The repairs for M5-R were more invasive, with replacement of concrete and reinforcement in all significantly damaged areas such that epoxy injection of cracks was not conducted. The repairs for M6-R were more isolated, with replacement of concrete and reinforcement only in the end regions and epoxy injection of cracks in the middle of the wall.

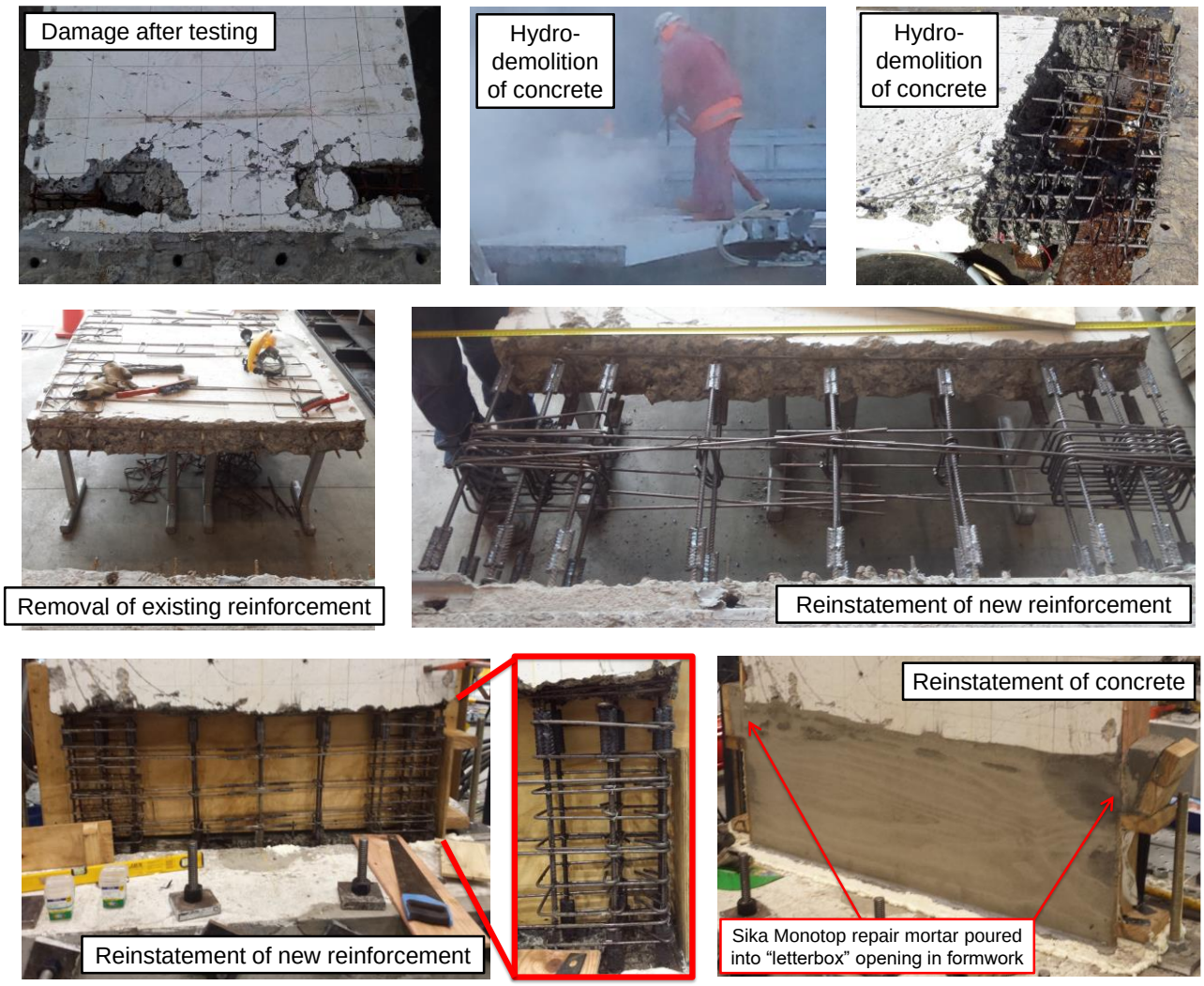

Figure 6: Repair procedure for wall M5-R.

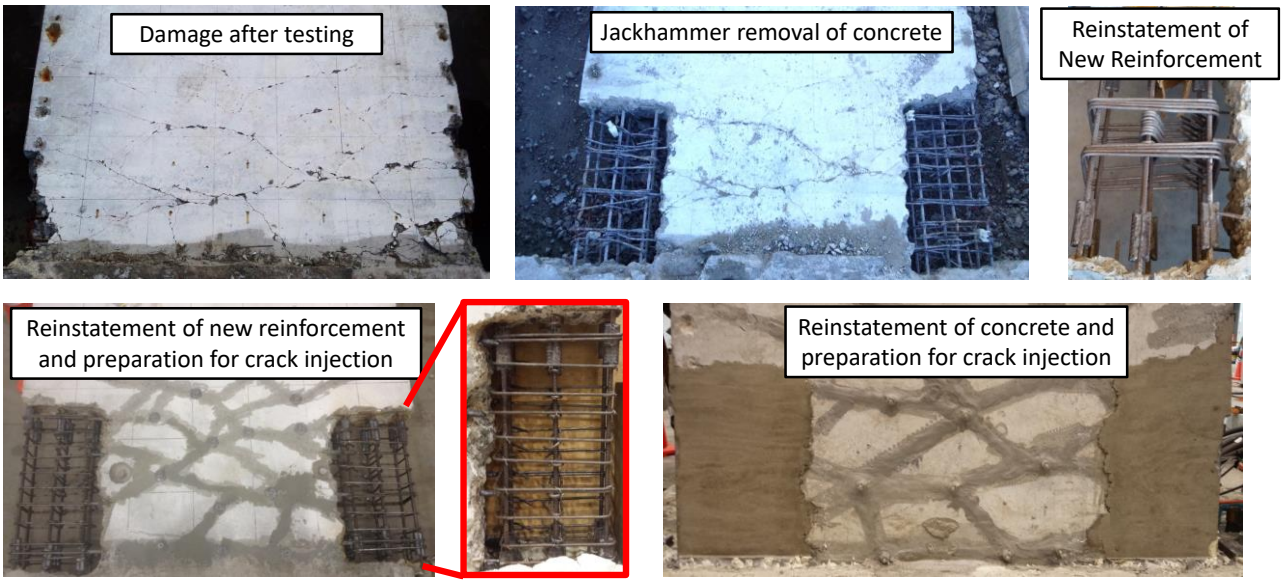

Figure 7: Repair procedure for wall M6-R.

An overview of the repair procedures for M5-R is shown in Figure 6. The repair process began by laying the wall flat and removing all of the concrete and reinforcement over a height of ~0.4l_w above the base of the wall, where l_w is the length of the wall. This distance was selected based on the extent of flexural cracking, such that the widths of any remaining cracks above the repair were too small for epoxy injection. Concrete was removed using hydro-demolition, a procedure in which a high-pressure jet of water is used to progressively break away concrete without damaging reinforcement. After completion of hydro-demolition, longitudinal reinforcement was cut near the top and bottom of the repaired region, with sufficient length of existing longitudinal reinforcement left in place to allow for welded connections to new segments of longitudinal

reinforcement. All reinforcement between the cuts was removed. The wall was then re-aligned and new segments of longitudinal reinforcement were installed using welded indirect butt splices to the existing longitudinal reinforcement near the top and bottom of the repaired region. The length of each welded segment was roughly 40 mm, such that the length of each splice bar was roughly 80 mm. All welded segments were above the beam-wall interface. Prior to welding these longitudinal bars, hoops and cross-ties at the wall end regions were positioned around the longitudinal bars and were then tied into position once the welding of the longitudinal reinforcement was complete. For constructability, the hoops that surrounded all of the longitudinal reinforcement in the original test specimens were replaced with overlapping U-bars that were welded with double lap splices over a length of at least 50 mm at both ends of the overlaps. Double lap splices were used here because yielding of this reinforcement was not expected. Once the reinforcement had been reinstated, the wall was positioned upright with strong-backs used to brace it during movement. Formwork was then installed around the repaired region. A letterbox opening was left in the formwork at each end of the wall such that repair mortar was poured through this opening. Reinstatement of the wall concrete using repair mortar completed the repair process. Crack injection was not conducted for this specimen due to the small crack widths above the repaired region.

An overview of the repair procedures for M6-R is shown in Figure 7. As the damage for M6 was less extensive than for M5 at the completion of testing, repair began by laying the wall flat and jackhammering to remove concrete only at the wall end regions over a height of ~0.4l_w. This height was selected to be consistent with M5-R. The transverse reinforcement and segments of the six longitudinal bars located at each of the two end regions were then removed and reinstated using the same procedure that was used for M5-R, except that existing horizontal web reinforcement was cut near the edge of the repaired region and U-bars were overlapped and welded with single lap splices (per [13]) over a length of at least 50 mm at the ends of the overlaps. Because shear yielding was not expected, single lap splices were used for these welds for ease of construction. Cracks at the centre region of the wall were prepared for injection, and the wall was then positioned upright. Formwork was installed and repair mortar reinstated using the same method used for M5-R. Epoxy injection of cracks completed the repair.

While both M5-R and M6-R were oriented in the vertical position during the pouring of repair mortar, the walls were lying flat without application of gravity load during much of the repair process. This was done to facilitate repair in the laboratory environment and is unrepresentative of conditions in an actual structure. In an actual structure, as shown in Figure 1, propping can be installed next to the wall in order to relieve the wall from gravity load while conducting this type of repair. Residual deformation could be removed prior to repair, if desired. Hence, the repairs used for M5-R and M6-R are considered realistic for application in practice. For both M5-R and M6-R repair did not extend into the foundation. Replacement of concrete and reinforcement could be extended into the foundation for cases in which fracture of reinforcement occurred at the wall-foundation interface. However, the repair approach used here is intended to restore previous performance and is not sufficient for cases of non-ductile response.

During reinstatement of concrete for each specimen, cylinders of the repair mortar were cast. Compression testing of these cylinders was conducted on the days that the specimens were tested to failure, with results shown in Table 2. The average repair mortar compressive strength was 35.0 MPa for M5-R, tested 25 days after casting, and 32.2 MPa for M6-R, tested 17 days after casting. For comparison, the average concrete compressive strength was 31.2 MPa for M5 and 29.0 MPa for M6. To obtain strain data, extensometers were installed on two of the cylinders tested for M6-R. In Figure 8, the stress-strain plot for these two cylinders is shown along with that of the concrete cylinder tests conducted on test days of the original M5 and M6 walls. In comparing the stress-strain plots, the repair mortar has a slightly lower stiffness than that of the concrete but was comparable in strength.

Table 2: Compressive strength of concrete and repair mortar.

Spec. Name	Material	Age (days)	Compressive Strength (MPa)					
			Cylinder Tests					Avg.
M5	Concrete	306	29.8	31.1	32.7	NA	NA	31.2
M6	Concrete	305	27.2	27.0	32.8	NA	NA	29.0
M5-R	Repair mortar	25	34.1	36.1	35.6	34.6	34.7	35.0
M6-R	Repair mortar	17	33.1	32.1	31.2	32.4	NA	32.2

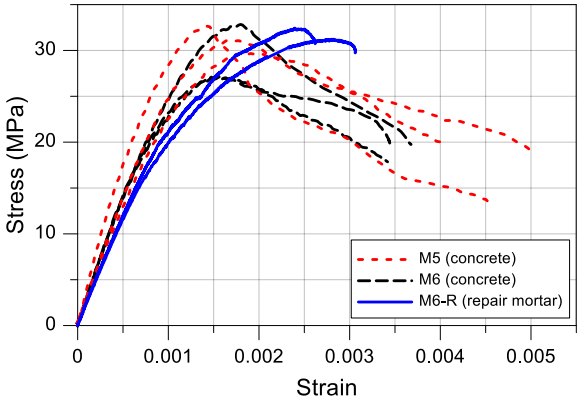

Figure 8: Stress-strain for concrete and repair mortar.

TEST SET-UP

Testing was conducted at the University of Auckland Structures Testing Laboratory. The test set-up, shown in Figure 9, followed that used for testing of M5 and M6 and reported by Lu et al [15] and Lu [14]. The specimen was post-tensioned to the laboratory strong floor, and a loading beam was attached to the top of the specimen. Two vertically-oriented actuators were attached to the loading beam and were used to apply constant axial load to the specimen. One horizontally-oriented actuator, attached to the laboratory strong wall at one end and to the end of the loading beam at the other end, was used to apply lateral load to the specimen. Based on the location of the horizontal actuator, the effective cantilever height of the wall was 2975 mm, corresponding to a shear span ratio (h/l_w) of 2.125. A steel frame was used to provide out-of-plane restraint at the top of the specimen during testing and to support the vertically orientated actuators, as shown in Figure 9.

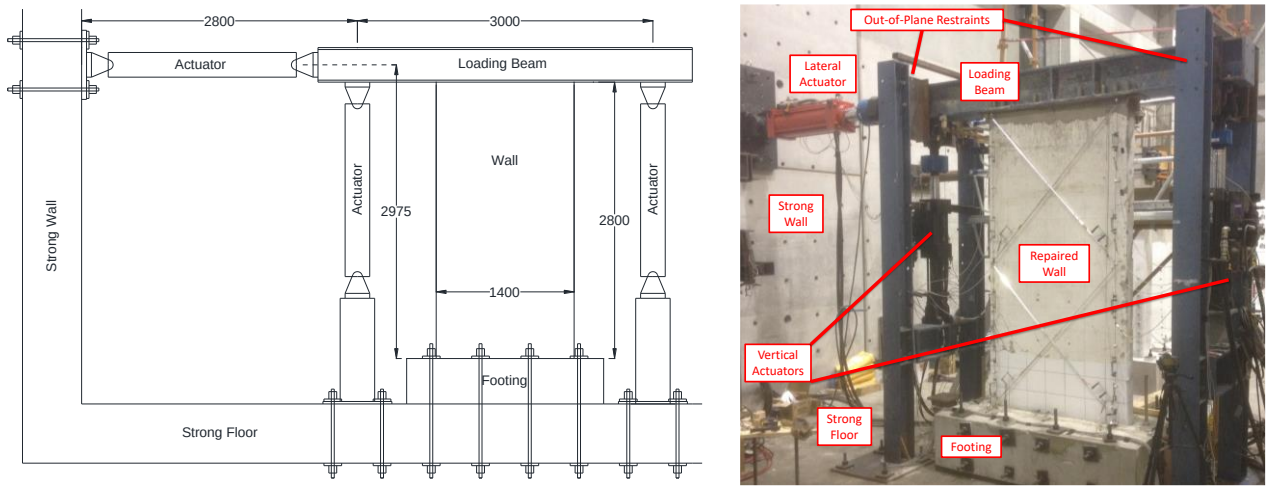

(a) (b)

Figure 9: Test set-up: a) schematic (dimensions in mm); b) photo.

TESTING PROTOCOL

Prior to the application of reversed-cyclic lateral load, axial load was applied and was maintained at a constant value of 294 kN throughout testing. For M5, M6, M5-R, and M6-R this axial load corresponded to $0.045A_g f'_{c,test}$, $0.048A_g f'_{c,test}$, $0.040A_g f'_{c,test}$, and $0.043A_g f'_{c,test}$, respectively, where A_g is the gross cross-sectional area of the wall and $f'_{c,test}$ is the tested compressive strength of the concrete (for M5 and M6) or repair mortar (for M5-R and M6-R) on test day. The test was drift-controlled based on the displacement measured at the location of lateral load application. The testing protocol for M5-R and M6-R, shown in Figure 10, consisted of a single force-controlled cycle at 25 kN, 50 kN, 75 kN, and 100 kN, followed by three displacement-controlled cycles at 0.20%, 0.25%, 0.35%, 0.50%, 0.75%, 1.0%, 1.5%, 2.0%, 2.5%, and 3.5% lateral drift. The loading protocol used for testing of M5 was developed by Lu [14] in accordance with ACI 374.2R-13 [16] and ACI ITG-5.1-07 [17] and was identical with that used for testing of M5-R except that the first four cycles of M5 were force-controlled at increments of 1/4, 1/2, 3/4 and 1 times the lateral load corresponding to the theoretical cracking moment at the base of the wall. The testing protocol used for M6, which was based on an analytically-determined response of the wall to an earthquake, was not used for testing of M6-R in favour of the quasi-static protocol shown in Figure 10. Use of the same testing protocol for both of the repaired specimens, M5-R and M6-R, enabled direct comparison between the performance of the two specimens to assess the impact that differences in the extent of previous damage and repair techniques had on performance.

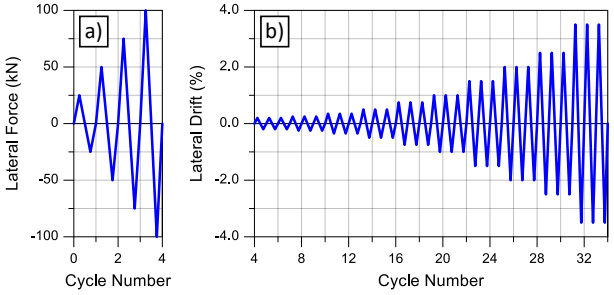

Figure 10: Testing protocol for M5-R and M6-R: a) force-controlled; b) displacement-controlled.

TEST RESULTS

In many instances, discussion in this section is limited in scope to specimens M5, M5-R, and M6-R, as the similarity in testing protocol for these three specimens enables direct assessment of the effectiveness of the repair techniques. The different loading protocol used for M6 makes direct comparison with the other specimens less relevant for the objectives of this study.

Observed Damage

The cycles at which damage states were first observed in specimens M5, M5-R, and M6-R are shown in Table 3. While some variation is evident in the load at cracking, similar cracks patterns developed for the repaired walls and the original wall, shown in Figure 11 and Figure 12, indicating that the crack pattern was not altered by the use of welded connections and repair mortar. At the peaks of pre-yield cycles, the widths of existing cracks above the repaired region for M5-R and M6-R were observed to open; however, for post-yield cycles, crack widths primarily increased in the repaired region, indicating plastic hinge formation at the base of the wall. Spalling did not occur in any of the specimens prior to 1.5% drift, and the spalling that occurred for M5 in the negative loading direction at 1.5% drift was believed to have been influenced by pre-existing damage to cover concrete that occurred during installation of instrumentation [14]. In all other instances, spalling of concrete did not initiate until the first cycle at 2.0% drift. For the repaired specimens, buckling of the longitudinal reinforcement occurred at the same cycle in which spalling initiated. For M5, buckling occurred two cycles later than spalling in both the positive and negative loading directions. For all three specimens, fracture of the longitudinal reinforcement was first observed during the third cycle at 2.0% drift or during one of the first two cycles at 2.5% drift.

While significant discrepancies in the initiation of damage states are not evident between the repaired walls and the original wall (Table 3), there were notable differences in the progression of damage. During the third cycle at 2.0% drift for M5-R, significant out-of-plane movement of the wall above the damaged region was observed (Figure 13). This behaviour was not observed for M5 and M6-R. After the completion of all cycles at 2.5% drift, five of the six longitudinal bars were fractured at each end region of M5-R, while damage was asymmetric for M6-R, with fracture of all six longitudinal bars at one end region and fracture of only two longitudinal bars at the other end region. Axial

compression failure occurred for M5-R during the first cycle at 3.5% drift in the negative direction (Figure 12), and the test was stopped. Axial compression failure did not occur for M5 and M6-R, resulting in less damage at the completion of testing than for M5-R (Figure 12). For all three specimens, damage concentrated at the base of the wall. No significant damage at the construction joint between concrete and repair mortar was observed for the repaired specimens. A general observation was made during testing that the repair mortar appeared to be more prone to crushing than concrete, perhaps due to the lack of large aggregate. This is consistent with the results of the cylinder tests shown in Figure 8, where less ductility is observed for the repair mortar.

Table 3: Cycle at which damage state was first observed.

Spec.	Dir.	Cracking	Spalling	Reinf. Buckling	Reinf. Fracture
M5	+	0.2% (1st) [1]	2.0% (1st)	2.0% (3rd)	2.0% (3rd)
	-	0.2% (1st) [2]	1.5% (1st)	1.5% (3rd)	2.5% (2nd)
M5-R	+	100 kN (1st)	2.0% (1st)	2.0% (1st)	2.0% (3rd)
	-	100 kN (1st)	2.0% (1st)	2.0% (1st)	2.5% (1st)
M6-R	+	100 kN (1st)	2.0% (1st)	2.0% (1st)	2.5% (1st)
	-	75 kN (1st)	2.0% (1st)	2.0% (1st)	2.5% (1st)

[1] Peak load of +163 kN (+82 kN for previous cycle).

[2] Peak load of -151 kN (-82 kN for previous cycle).

(a) (b) (c)

Figure 11: Damage photos at 0.35% drift: a) M5; b) M5-R; c) M6-R.

(a) (b) (c)

Figure 12: Damage photos after completion of tests: a) M5; b) M5-R; c) M6-R.

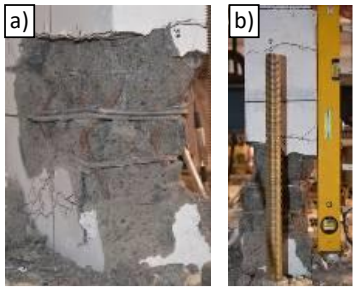

Figure 13: M5-R at -2.0% drift, 3rd cycle: a) buckling of longitudinal reinforcement; b) out-of-plane movement.

Load-Deformation Response

The load-deformation responses for the repaired walls, M5-R and M6-R, are compared against that of the original walls, M5 and M6, in Figure 14. The elastic stiffness of the repaired walls was lower than that of the unrepaired walls, with details provided in the next section. Except for M6 in the negative loading direction, peak lateral load strengths, V_{max}, among the tests were within 10% difference for all cases (see Table 4). For M5, M5-R, and M6-R, significant strength degradation and pinching in the load-deformation response in Figure 14 was not evident through the completion of the first loading cycle at 2.0% drift. The similarity in the load-deformation responses up to this drift level indicates that it is feasible to achieve acceptable performance of severely-damaged lightly-reinforced concrete walls repaired through replacement of reinforcement and concrete in the damaged region. During subsequent loading cycles at 2.0% drift, 2.5% drift, and 3.5% drift, larger cyclic degradation was evident for M5-R compared to M6-R and M5, while cyclic degradation for M6-R was similar to M5 in the positive direction but larger in the negative direction. The more rapid strength degradation for M5-R relative to M6-R and M5 may have been influenced by the out-of-plane movement of M5-R, as shown in Figure 13. The drift at lateral failure, $\Delta_{failure}$, of M5-R was less than that of M6-R and M5, as shown in Table 4. Lateral failure was defined to occur when the load at a cycle peak dropped below 80% of the maximum load and did not return to this value. For M5-R, axial failure occurred when loading to the first cycle at 3.5% drift in the negative direction. For M6-R and M5, axial failure did not occur, and three loading cycles were completed at 3.5% drift.

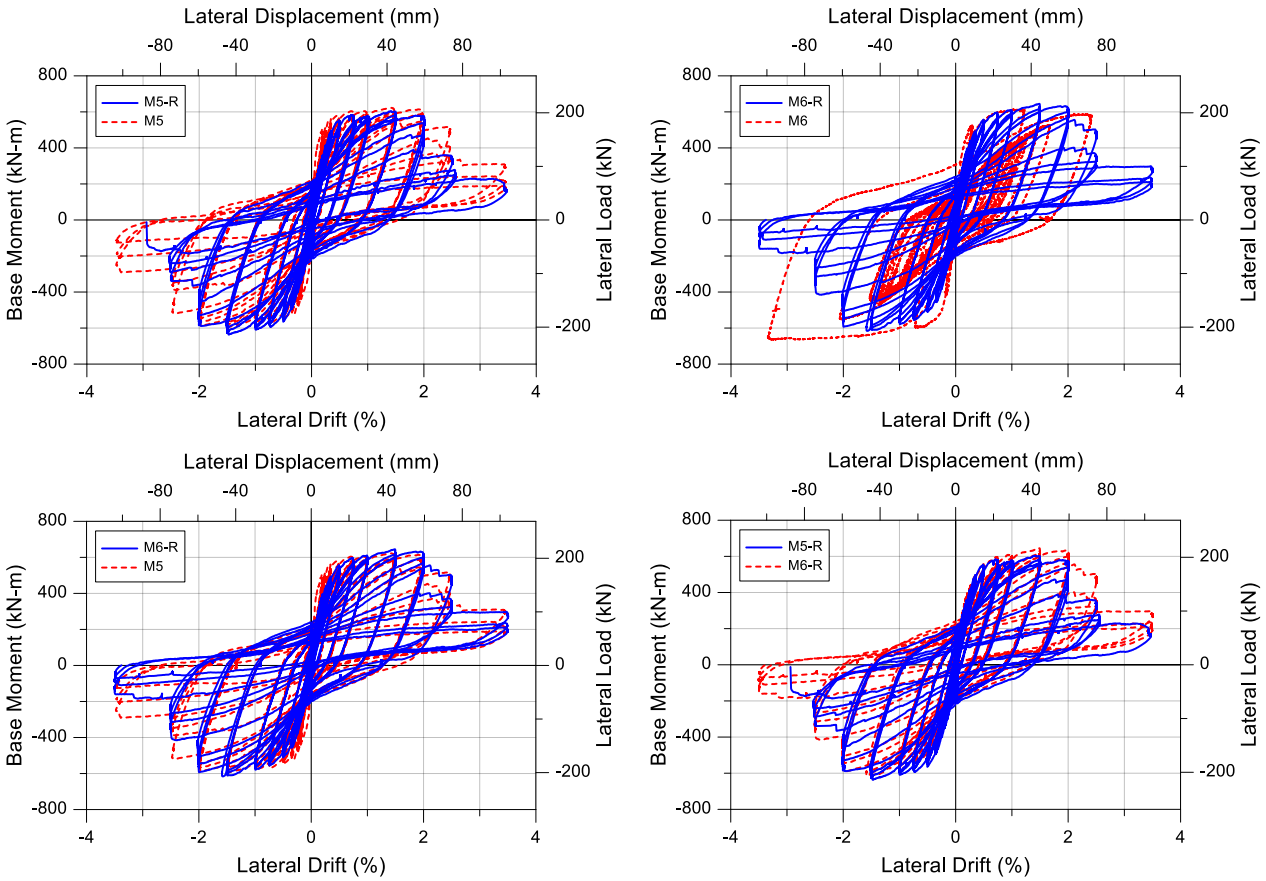

Figure 14: Load-deformation responses of repaired walls (M5-R and M6-R) and original walls (M5 and M6).

Table 4: Peak lateral load and drift at lateral failure.

	M5		M6		M5-R		M6-R	
	(+)	(-)	(+)	(-)	(+)	(-)	(+)	(-)
V_{max}	209.2 kN	199.2 kN	206.5 kN	223.2 kN	202.9 kN	213.9 kN	216.9 kN	207 kN
$\Delta_{failure}$	2.5% (2nd cycle)	2.5% (2nd cycle)	N.A.	N.A.	2.0% (3rd cycle)	2.0% (3rd cycle)	2.5% (1st cycle)	2.5% (1st cycle)

Sources of Deformation

The walls tested in this study failed in flexure, as the ratio of nominal shear strength, V_n, to shear at nominal flexural strength, $V@M_n$, was 1.74 for these walls. The peak lateral loads shown in Table 4 correspond to shear stress demands of ~$0.19\sqrt{f_c'}$, and diagonal cracking occurred due to shear (see Figure 11 and Figure 12). The plots in Figure 15 show the sources of deformation as a function of drift and were formulated using data points at the peaks of initial loading cycles at each drift level. In these plots, flexural deformations include reinforcement slip/extension at the wall-to-foundation interface and shear deformations include sliding at the wall-to-foundation interface. The shear deformations above the wall-to-foundation interface were measured using diagonally-oriented sensors and were corrected for flexure. The "other/error" sources of deformation represent the remainder obtained when subtracting the sum of the contributions from flexure and shear deformation from the overall deformation. It is evident from the plots in Figure 15 a) and b) that flexural deformations were responsible for the majority of the overall deformation, accounting for at least 75% of the deformation except for cycles at 0.20% drift or less in the negative loading direction for M5-R. Shear deformations accounted for less than 10% of the overall deformation in all instances, with the exception of cycles at 0.5% drift or less for M5-R in the negative loading direction where the shear deformations accounted for between 15% and 10% of the total deformation. The "other/error" sources of deformation did not exceed 20% of the total drift and, with the exception of M5 in the negative loading direction, were less than 10% of the total drift for all cycles beyond 0.35% drift. The sources of deformation for M5-R and M6-R were similar to those for M5 (Figure 15c), where flexural deformation accounted for more than 70% of the total deformation and shear deformation accounted for less than roughly 10% of the total deformation. Therefore, the repairs did not lead to a significant change in the components of deformation. However, a change in the distribution of flexural deformation over the height of the wall is evident in Figure 16 for M5-R and M6-R relative to M5, with the region above the repair accounting for a larger percentage of the total deformation.

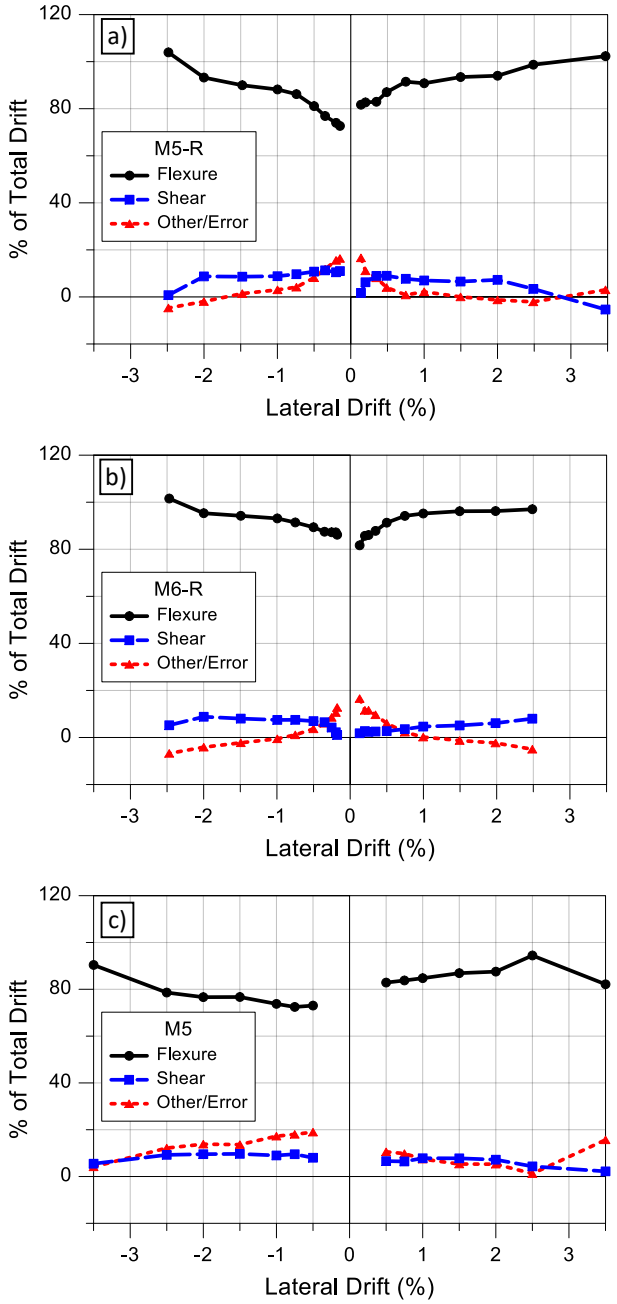

Figure 15: Sources of deformation for a) M5-R, b) M6-R, and c) M5.

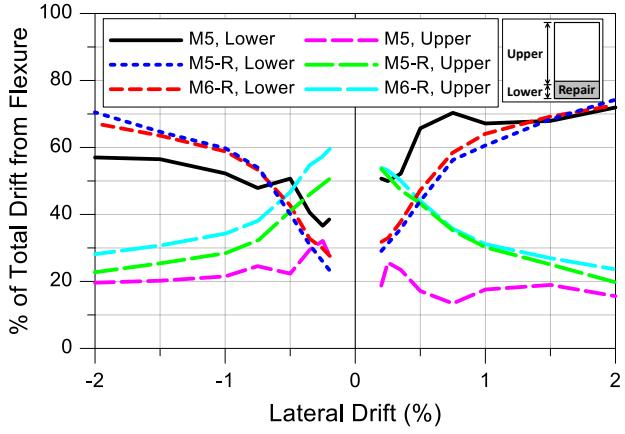

Figure 16: Flexural contribution to deformation.

Backbones and Effective Stiffness

For M5, M5-R, and M6-R, backbone load-deformation responses for initial loading cycles at each drift level are provided in Figure 17. The elastic stiffness of M5-R and M6-R was lower than that of M5, but the post-yield plateaus of the three backbones were similar through 2.0% drift. Beyond 2.0% drift, strength degradation was largest for M5-R, while strength degradation for M6-R matched that of M5 in the positive direction and is larger in the negative direction. Values for the measured effective secant stiffness, $(EI)_{sec}$, at peaks of first cycles in both the positive and negative loading directions are plotted versus drift in Figure 18. Wall stiffness was modelled entirely as bending stiffness and is normalized by E_cI_g, where E_c is the modulus of elasticity of concrete computed as $E_c = 4700\sqrt{f_c'}$ (per [18]) and I_g is the gross moment of inertia of the concrete section. Modelling of the effective stiffness as bending stiffness reflects a lumped deformation modelling approach in which all of the deformation is attributed to bending. This approach was deemed appropriate, given that shear deformation accounted for less than 15% of the total deformation in the elastic range for M5-R, M6-R, and M5 (see Figure 15). Within the elastic range, significant variation is evident in the effective secant stiffness, as shown in Figure 18. Therefore, an effective elastic stiffness, $(EI)_{eff}$, was estimated for each test in both the positive and negative loading directions based on the force and drift coordinates of a point located on the backbone curve at 75% of the peak load. The resulting effective elastic stiffness values (shown in Figure 17) for M5 were $0.25E_cI_g$ and $0.29E_cI_g$, while the values for the repaired walls were roughly 33-50% lower at ~$0.15E_cI_g$. The effective elastic stiffness values for M5-R and M6-R were similar, meaning that the differences in the repair techniques did not lead to significant differences in stiffness. It is evident from Figure 19 that the original stiffness was restored in the repaired regions, with the exception of a modest reduction in stiffness for M6-R in the negative loading direction that is consistent with the lower observed load at cracking (see Table 3). The original stiffness was not restored above the repairs (Figure 19), leading to the increased deformation above the repairs evident in Figure 16. For the walls tested in this study, it is appropriate to model an effective elastic stiffness value that is 50% of that of the original wall in unrepaired zones, with the full stiffness value used in repaired zones. This leads to a 41% reduction in the overall stiffness for M5-R and M6-R relative to M5 based on the repair height of $0.4l_w$. An equivalent effective elastic stiffness (i.e., a single value) could be determined for the full-height wall for use in modelling software.

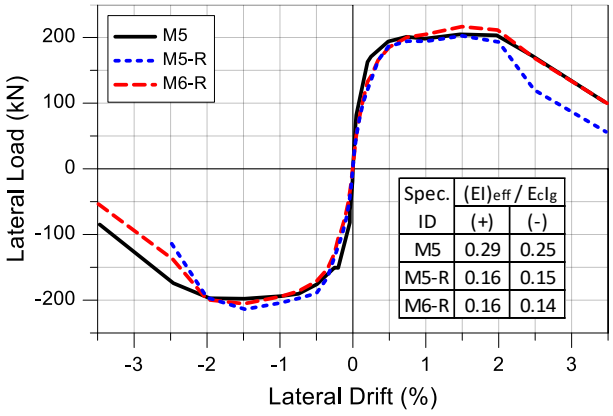

Figure 17: Backbones.

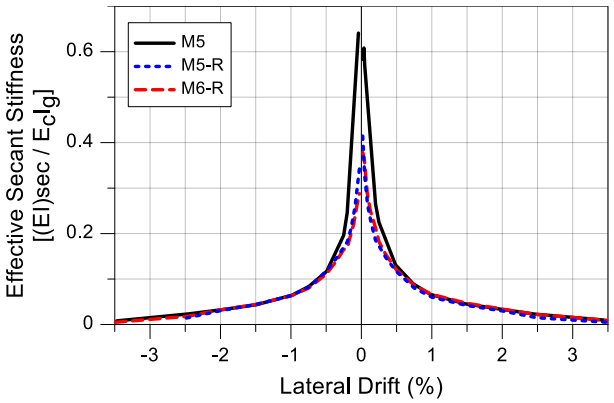

Figure 18: Effective secant stiffness.

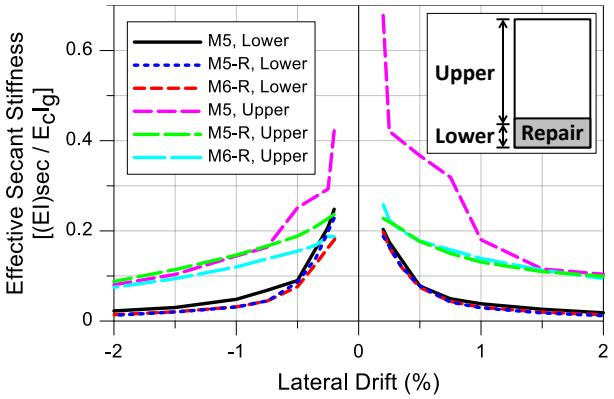

Figure 19: Effective secant stiffness in lower and upper regions.

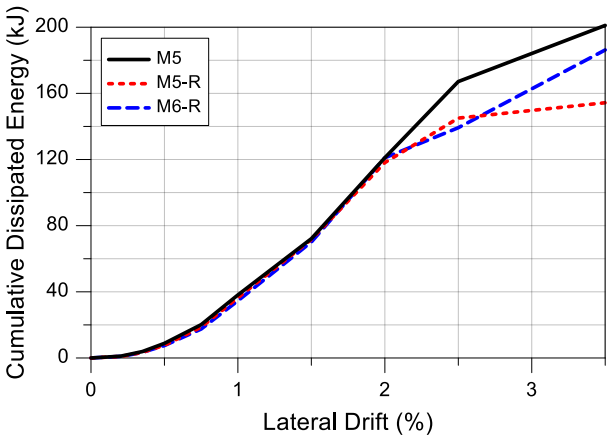

Figure 20: Dissipated energy.

Dissipated Energy

Dissipated energy was calculated based on the area bounded by hysteretic loops in the load-deformation plots in Figure 14. A plot of the cumulative dissipated energy at the completion of all cycles up to and including the given drift level is shown in Figure 20. It is evident that the dissipated energy of both repaired walls, M5-R and M6-R, was almost identical to that of the original wall, M5, up to and including 2.0% drift. Therefore, the reduced stiffness of the repaired walls relative to the original walls (Figure 17 and Figure 18) and the increased cyclic degradation in the load-deformation response that occurred during the three cycles at 2.0% drift for M5-R relative to M6-R and M5 (Figure 14) did not have a significant impact on the cumulative energy dissipated through 2.0% drift. For drift demands beyond 2.0%, a decrease in dissipated energy was observed for M5-R and M6-R relative to M-5.

SUMMARY AND CONCLUSIONS

Two previously tested lightly-reinforced concrete walls were repaired and retested to assess the performance of the repaired walls, M5-R and M6-R, relative to the original walls, M5 and M6, and relative to one another. The two walls had different levels of damage prior to repair. The damage prior to repair included buckling and fracture of longitudinal reinforcement, crushing and spalling of concrete, and, for one of the specimens (M5), out-of-plane instability of the gross section. Prior to repairing the specimens, tensile testing of reinforcement connections was conducted to verify acceptable performance. Concrete and reinforcement were replaced over the full plastic hinge for M5-R versus just at the end regions of the plastic hinge for M6-R. Welded connections were used to install the new vertical reinforcement, and repair mortar was used in place of concrete. The repaired walls, M5-R and M6-R, were tested under an identical loading protocol that was consistent with that used for one of the original specimens, M5. Aside from a lower elastic stiffness, the load-deformation responses of the repaired walls, M5-R and M6-R, and the original wall, M5, were very similar through the first loading cycle at 2.0% drift. Lateral failure, taken as a 20% loss in lateral load carrying capacity, occurred during the third cycle at 2.0% drift for M5-R, the first cycle at 2.5% drift for M6-R, and the second cycle at 2.5% drift for M5.

The following conclusions were reached for the repair of lightly-reinforced concrete walls (although it is noted that these conclusions are based on limited testing and further research is recommended):

1. The similarity in load-deformation response for M5-R, M6-R, and M5 through the first cycle at 2.0% drift indicates that it is feasible to achieve favourable performance of severely-damaged lightly-reinforced concrete walls repaired through replacement of reinforcement and concrete in the damaged region. Reinforcement in damaged regions can be removed, and new reinforcement may then be successfully reinstated with indirect butt splice welds. Damaged concrete in the wall regions may be removed and replaced with repair mortar. These repair techniques allow for formation of the plastic hinge at the base of the wall, consistent with the behaviour in an undamaged wall.
2. Repairs based on the level of observed damaged are appropriate. At wall end regions where core concrete has crushed or longitudinal reinforcement has buckled or fractured, replacement of reinforcement and concrete is suggested along the full length of the wall end region and over the height in which yielding was observed (i.e., the height over which crack openings large enough for epoxy injection are observed). If spalling of concrete is not observed in the web, repairs in the web may be limited to epoxy injection of cracks.
3. As flexural deformation generally accounted for over 80% of the elastic deformation, the use of a lumped deformation modelling approach with an effective bending stiffness is suggested. The effective elastic stiffness in the repaired walls was roughly $0.15E_cI_g$, which was 33-50% lower than that of the original wall, M5. Stiffness was restored in regions where concrete and reinforcement were repaired but not in unrepaired regions. For the walls tested in this study, modelling an effective elastic stiffness that is 50% of that used for the original wall is appropriate in the unrepaired regions, while the full value may be used in repaired regions, as this led to a 41% reduction in overall stiffness. An equivalent effective elastic stiffness (i.e., a single value) can be determined for the full-height wall for use in modelling software.

ACKNOWLEDGEMENTS

This project was partially supported by the New Zealand Centre for Earthquake Resilience (QuakeCoRE), a New Zealand Tertiary Education Commission-funded Centre. This is QuakeCoRE publication number 0115. In addition, the repairs were performed on walls that were part of a previous research project funded by the Building Systems Performance branch of the Ministry of Business, Innovation, and Employment (MBIE). Significant in-kind contributions from Sika, Complete Reinforcement, Aquamax Hydroblasting, BBR Contech, and Fulton Hogan are also gratefully acknowledged. Yiqiu Lu is thanked for design of the test setup and the original test specimens and for testing and providing test data for M5. Ronald Gultom is thanked for assistance with testing of M5-R and M6-R and for testing and providing test data for M6. The authors would additionally like to acknowledge the support of the lab technical staff at the University of Auckland, namely Felix Scheibmair, Ross Reichardt, Jay Naidoo, Shane Smith, Andrew Virtue, and Mark Byrami. Support for the fourth author was provided through the Fondecyt Grant #1171062. Information on damaged buildings in Viña del Mar, Chile that was provided by Patricio Bonelli and Jorge Carvallo is greatly appreciated.

REFERENCES

1 Marquis F, Kim JJ, Elwood KJ and Chang SE (2017). "Understanding Post-Earthquake Decisions on Multi-Storey Concrete Buildings in Christchurch, New Zealand". *Bulletin of Earthquake Engineering*, **15**(2): 731-758.

2 Rodriguez M, and Park R (1991). "Repair and Strengthening of Reinforced Concrete Buildings for Seismic Resistance". *Earthquake Spectra*, **7**(3): 439-459.

3 Cuevas A and Pampanin S (2017). "Post-Seismic Capacity of Damaged and Repaired Reinforced Concrete Plastic Hinges Extracted from a Real Building". *Proceedings of the 16th World Conference on Earthquake Engineering* (16WCEE), Santiago, Chile.

4 Marder KJ, Elwood KJ and Clifton GC (2017). "Post-Earthquake Residual Capacity of Damaged Reinforced Concrete Buildings". *Proceedings of the 16th World Conference on Earthquake Engineering* (16WCEE), Santiago, Chile.

5 Kam WY, Pampanin S and Elwood K (2011). "Seismic Performance of Reinforced Concrete Buildings in the 22 February Christchurch (Lyttelton) Earthquake". *Bulletin of the New Zealand Society of Earthquake Engineering*, **44**(4): 239-278.

6 Elwood KJ (2013). "Performance of Concrete Buildings in the 22 February 2011 Christchurch Earthquake and Implications for Canadian Codes". *Canadian Journal of Civil Engineering*, **40**(8): 759–776.

7 Sritharan S, Beyer K, Henry RS, Chai YH, Kowalsky M and Bull D (2014). "Understanding Poor Seismic Performance of Concrete Walls and Design Implications". *Earthquake Spectra*, **30**(1): 307-334.

8 Wallace JW, Massone LM, Bonelli P, Dragovich J, Lagos R, Lüders C and Moehle J (2012). "Damage and Implications for Seismic Design of RC Structural Wall Buildings". *Earthquake Spectra*, **28**(S1): S281–S299.

9 Westenenk B, de la Llera JC, Jünemann R, Hube MA, Besa JJ, Lüders C, Inaudi JA, Riddell R and Jordán R (2013). "Analysis and Interpretation of the Seismic Response of RC Buildings in Concepción during the February 27, 2010, Chile Earthquake". *Bulletin of Earthquake Engineering*, **11**(1): 69-91.

10 Marquis F (2015). "*A Framework for Understanding Post-Earthquake Decisions on Multi-Storey Concrete Buildings in Christchurch, New Zealand*". Master's Thesis, University of British Columbia, Vancouver, Canada.

11 Carvallo JF and Alcaíno PE (2012). "Behavior of Reinforced Concrete Buildings in Viña del Mar: Lessons of February 27th 2010 Earthquake". *Proceedings of the 15th World Conference on Earthquake Engineering* (15WCEE), Lisbon, Portugal.

12 Sherstobitoff J, Cajiao P and Adebar P (2012). "Repair of an 18-Story Shear Wall Building Damaged in the 2010 Chile Earthquake". *Earthquake Spectra*, **28**(S1): S335-S348.

13 AS/NZS 1554.3 (2014). "*Structural Steel Welding Part 3: Welding of Reinforcing Steel*." Standards New Zealand, Wellington, New Zealand.

14 Lu Y (2017). "*Seismic Design of Lightly Reinforced Concrete Walls*". PhD Thesis, University of Auckland, Auckland, New Zealand.

15 Lu Y, Henry RS, Gultom R and Ma QT (2015). "Experimental Testing and Modelling of Reinforced Concrete Walls with Minimum Vertical Reinforcement". *Proceedings of the Annual Conference of New Zealand Society of Earthquake Engineering (NZSEE)*, Rotorua, New Zealand.

16 ACI 374.2R-13 (2013). "*Guide for Testing Reinforced Concrete Structural Element under Slowly Applied Simulated Seismic Loads*". American Concrete Institute, Farmington Hills, Michigan.

17 ACI ITG-5.1-07 (2008). "*Acceptance Criteria for Special Unbonded Post-Tensioned Precast Structural Walls Based on Validation Testing and Commentary*". American Concrete Institute, Farmington Hills, Michigan.

18 NZS 3101:2006 A3 (2017). "*Concrete Structures Standard Amendment 3*". Standards New Zealand, Wellington, New Zealand.